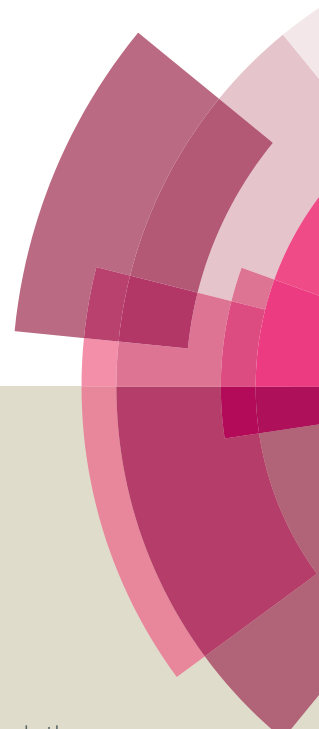


# Catalysis Science & Technology

Accepted Manuscript



This article can be cited before page numbers have been issued, to do this please use: I. Pardo, G. Santiago, P. Gentili, F. Lucas, E. Monza, F. J. Medrano, C. Galli, A. T. Martinez Ferrer, V. Guallar and S. Camarero, *Catal. Sci. Technol.*, 2015, DOI: 10.1039/C5CY01725D.



This is an *Accepted Manuscript*, which has been through the Royal Society of Chemistry peer review process and has been accepted for publication.

*Accepted Manuscripts* are published online shortly after acceptance, before technical editing, formatting and proof reading. Using this free service, authors can make their results available to the community, in citable form, before we publish the edited article. We will replace this *Accepted Manuscript* with the edited and formatted *Advance Article* as soon as it is available.

You can find more information about *Accepted Manuscripts* in the [Information for Authors](#).

Please note that technical editing may introduce minor changes to the text and/or graphics, which may alter content. The journal's standard [Terms & Conditions](#) and the [Ethical guidelines](#) still apply. In no event shall the Royal Society of Chemistry be held responsible for any errors or omissions in this *Accepted Manuscript* or any consequences arising from the use of any information it contains.

## ARTICLE

## RE-DESIGNING THE SUBSTRATE BINDING POCKET OF LACCASE FOR ENHANCED OXIDATION OF SINAPIC ACID

Received 00th January 20xx,  
Accepted 00th January 20xx

DOI: 10.1039/x0xx00000x

www.rsc.org/

I. Pardo,<sup>a</sup> G. Santiago,<sup>b</sup> P. Gentili,<sup>c</sup> F. Lucas,<sup>b,d\*</sup> E. Monza,<sup>b</sup> F. J. Medrano,<sup>a</sup> C. Galli,<sup>c</sup> A. T. Martínez,<sup>a</sup> V. Guallar,<sup>b,e</sup> and S. Camarero<sup>a\*</sup>

Iterative saturation mutagenesis was performed over six residues delimiting the substrate binding pocket of a high-redox potential chimeric laccase with the aim of enhancing its activity over sinapic acid, a lignin-related phenol of industrial interest. In total, more than 15000 clones were screened and two selected variants, together with the parent-type laccase, were purified and characterized. The new variants presented shifted pH activity profiles and enhanced turnover rates on sinapic acid and its methyl ester, whereas the oxidation of related phenols was not significantly enhanced. Neither the enzyme's redox potential nor the mechanism of the reaction were affected. Quantum mechanics and molecular dynamics calculations were done to rationalize the effect of the selected mutations, revealing the critical role of the residues of the enzyme pocket to provide the precise binding of the substrate that enables an efficient electron transfer to the T1 copper. The results presented highlight the power of combining directed evolution and computational approaches to give novel solutions in enzyme engineering and to understand the mechanistic reasons behind them, offering new insights for further rational design towards specific targets.

## Introduction

Laccases are multi-copper oxidases capable of oxidizing a wide range of compounds, especially substituted phenols and aromatic amines, coupled to the reduction of molecular oxygen to water. Some laccases secreted by white-rot fungi involved in lignin degradation (typically belonging to the order Polyporales) stand out for their high-redox potential at the T1 copper site ( $E^0 \sim 0.8$  V), compared to laccases from other fungi, plants or bacteria (from 0.4 to 0.7 V). Moreover, the use of redox mediators, which are small molecules that can act as diffusible electron shuttles between the substrate and laccase, can further extend the oxidative capabilities of these enzymes. In previous studies we described the ability of certain phenolic compounds related to lignin to act as laccase mediators.<sup>1,2</sup> The combined application of laccase and these natural mediators might be a key factor for the integrated use of plant biomass in lignocellulosic biorefineries for the sustainable production of chemicals, materials and fuels.<sup>3,4</sup>

The potential of laccases as industrial biocatalysts has led to numerous efforts to engineer these enzymes with the aim of enhancing their activity and/or stability for industrial

application.<sup>5</sup> In this sense, directed evolution has proven to be a powerful tool to obtain laccases *a la carte*. In a previous work we described the construction of chimeric laccases by random DNA shuffling of two high-redox potential laccases (HRPLs) from basidiomycetes PM1 and *Pycnoporus cinnabarinus* expressed in *Saccharomyces cerevisiae*.<sup>6–8</sup> The new laccases presented improved properties with respect to both parent types, including better substrate affinities and increased stability towards temperature and pH.

Using one chimeric laccase (3A4) with increased affinity towards phenols as scaffold, we aim here to enhance its activity towards sinapic acid (SA). This *p*-hydroxycinnamic acid is of biotechnological interest for: a) its ability to act as laccase mediator; b) the biological activity (as antioxidant, antimicrobial, immunomodulatory, antitumoral or UV-B screening agents) of SA itself, its esters or other derivatives;<sup>2,9–12</sup> and c) the role of sinapate dehydrodimers or heterodimers (with ferulate) in cross-linking polysaccharides in grass cell walls. Indeed, *p*-hydroxycinnamic acids are one of the main inhibitory phenolic compounds released during physico-chemical pretreatment of lignocellulose for ethanol production. Detoxification of wheat straw slurries by laccase, after the enzymatic hydrolysis or during the simultaneous saccharification and fermentation, has been described to enhance yeast fermentation performance and raise the final ethanol yields,<sup>13,14</sup> allowing also to work at higher substrate consistencies.<sup>15</sup>

To this end, we describe here the re-design of the laccase's substrate binding pocket by iterative saturation mutagenesis (ISM)<sup>16</sup> of six residues limiting the cavity. This is the first time that the systematic exploration of all possible amino acid substitutions and their combinations is attempted in laccases, as compared to previous works.<sup>17–19</sup> At the same time we

<sup>a</sup> Centro de Investigaciones Biológicas, CSIC. Ramiro de Maeztu 9, 28040 Madrid, Spain.

<sup>b</sup> Joint BSC-CRG-IRB Research Program in Computational Biology, Barcelona Supercomputing Center, c/Jordi Girona 29, 08034 Barcelona, Spain.

<sup>c</sup> Dipartimento di Chimica, Università "La Sapienza" and IMC-CNR Sezione Meccanismi di Reazione, P.le A. Moro 5, 00185 Rome, Italy.

<sup>d</sup> Anaxomics Biotech, Balmes 89, E-08008 Barcelona, Spain.

<sup>e</sup> ICREA, Passeig Lluís Companys 23, 08010 Barcelona, Spain.

\* Corresponding authors: S.C. e-mail: susanacam@cib.csic.es; F.L. e-mail: fatima.lucas@bsc.es.

Electronic Supplementary Information (ESI) available: [details of any supplementary information available should be included here]. See DOI: 10.1039/x0xx00000x

address the biochemical and mechanistic characterization of two engineered laccase variants selected for their increased activity towards SA, together with the computational simulations performed to rationalize the effect of the inserted mutations.

## Experimental section

### Construction of mutant libraries

Sequences of laccases from basidiomycetes of the order Polyporales were retrieved from UniProt KB, filtering for a minimum length of 450 amino acids and clustering identical sequences. Selected sequences were aligned using T-Coffee<sup>20</sup> and sequence logos were generated with WebLogo 3<sup>21</sup> server. The most variable residues delimiting the substrate binding pocket (six in total) were selected for mutagenesis. Mutant libraries were obtained by IVOE,<sup>22</sup> using the pJRoC30 plasmid containing 3A4 coding sequence fused to an evolved alpha-factor pre-proleader as template.<sup>8</sup> Complementary mutagenic primers were designed so that degenerate codons (NNK, where N = A/C/G/T, and K = G/T) were flanked by ~20 bp (Table S1). For each mutagenesis site two PCRs were performed: one with RMLN and the reverse mutagenic primer, and another with RMLC and the forward mutagenic primer. RMLN and RMLC primers anneal with pJRoC30 plasmid, flanking the  $\alpha$ -3A4 CDS. PCR conditions, product purification and in vivo cloning in competent *S. cerevisiae* BJ5465 cells have been described previously.<sup>8</sup>

### Screening of mutant libraries

For each mutant library, at least 3066 clones were analyzed in order to obtain 95 % library coverage (two positions with NNK degeneracy). Culture media for cell growth and laccase expression in 96-well plates, and the general procedure for library screening and the two re-screenings are described previously.<sup>7,8</sup> In this work, libraries were screened for activity towards 250  $\mu$ M SA (at 512 nm) in 100 mM acetate buffer, pH 5.<sup>7,23</sup> A thermostability screening assay was also performed with some selected clones.<sup>24</sup>

### Production and purification of mutated laccases

Individual colonies of selected clones were grown in minimal medium (6.7 g/L YNB, 1.92 g/L drop-out media supplements without uracil, 2 % raffinose and 25 mg/L chloramphenicol) for 48 h at 30 °C, and 220 rpm. Aliquots of these cultures were used to inoculate 30 mL of minimal medium in 250 mL flasks to an OD<sub>600</sub> = 0.25, which were incubated until an OD<sub>600</sub> = 1 was reached. Then, cells were diluted tenfold to a final volume of 300 mL with laccase expression minimal medium (6.7 g/L YNB, 1.92 g/L drop-out media supplements without uracil, 2 % galactose, 67 mM phosphate buffer, pH 6, 1 mM CuSO<sub>4</sub>, and 25 mg/L chloramphenicol) in 1 L flasks. Cultures were grown at 30 °C, 220 rpm, until maximum laccase activity was reached (3–4 days). Standard laccase activity assay consisted in measuring the oxidation of 3 mM 2,2'-azino-bis(3-ethylbenzothiazoline-6-sulfonic acid) (ABTS) in 100 mM acetate buffer (pH 5) in the

spectrophotometer (ABTS<sup>+</sup>,  $\epsilon_{418}$  = 36000 M<sup>-1</sup> cm<sup>-1</sup>), defining one unit of laccase as the amount of enzyme needed to transform 1  $\mu$ mol ABTS per minute.

Cultures were centrifuged at 10000  $\times$  g for 15 min at 4 °C, and supernatants were consecutively filtered through 0.8 and 0.45  $\mu$ m pore-size membranes. Then, crude extracts were concentrated by ultra-filtration through 10000 MWCO membranes and dialyzed against 20 mM Tris-HCl buffer, pH 7. Laccases were purified by HPLC (AKTA purifier, GE Healthcare) in two anion-exchange and one molecular exclusion steps: first, using a HiPrep Q FF 16/10 column and a 100 mL gradient of 0 – 40 % elution buffer (20 mM Tris-HCl + 1 M NaCl, pH 7); second, using a Mono Q HR 5/5 column and a 30 mL gradient of 0 – 25 % elution buffer; and finally using a HiLoad 16/600 Superdex 75 pg column and 20 mM Tris-HCl + 150 mM NaCl, pH 7 (all columns from GE Healthcare). Fractions containing laccase activity were pooled, dialyzed and concentrated between each chromatographic step.

### Biochemical characterization of laccase variants

Microplate assays to determine T<sub>50</sub> (10 min), pH activity profiles, and kinetic constants of purified laccase variants are described previously.<sup>7</sup> Kinetic constants for SA ( $\epsilon_{312}$  = 17600 M<sup>-1</sup> cm<sup>-1</sup>), methyl sinapate (MS,  $\epsilon_{320}$  = 18855 M<sup>-1</sup> cm<sup>-1</sup>) and 2,6-dimethoxyphenol (DMP, product  $\epsilon_{469}$  = 27500 M<sup>-1</sup> cm<sup>-1</sup>, referred to DMP concentration) were determined in 96-well plates, using UV-transparent microplates for SA and MS (UV-Star, Greiner Bio-One). Kinetic constants for dehydrodisinapic acid dilactone (DAD, product  $\epsilon_{530}$  = 17000 M<sup>-1</sup> cm<sup>-1</sup>, referred to DAD concentration) were determined in the spectrophotometer using 1 cm path-quartz cuvettes. In the case of syringic acid (SyA,  $\epsilon_{260}$  = 9035 M<sup>-1</sup> cm<sup>-1</sup>) and methyl syringate (MSy,  $\epsilon_{275}$  = 11660 M<sup>-1</sup> cm<sup>-1</sup>), reactions were carried out in 0.1 cm path-quartz cuvettes. Due to the high initial absorbance of MSy, reactions for higher concentrations (mM range) were followed discontinuously, taking aliquots at different time-points and diluting 10-fold prior to measuring A<sub>275</sub>. The chemical structure of phenolic compounds for which kinetic constants were obtained are shown in Fig. S1.

Competition reactions with *p*-X-substituted phenols were carried out as described previously,<sup>25</sup> with slight modifications: 2 or 5 units of the different variants were added to a 600  $\mu$ L mixture of O<sub>2</sub>-saturated 100 mM citrate buffer (pH 5) and dioxane (v:v ratio 2:1) containing 6  $\mu$ mol of each phenolic substrate. Reactions proceeded at room temperature with stirring and under O<sub>2</sub> atmosphere. After addition of 4-methoxyacetophenone as internal standard and extraction with ethyl acetate, consumption of substrates at end-point was determined with an Agilent 6850 Series II GC equipped with a methyl silicone capillary column. Hammett plots were obtained by representing relative reaction constants log( $k_x/k_H$ ) versus  $\sigma^+$  for the different *p*-X-substituted phenols and fitting to a straight line.

Redox potentials of the different variants were determined by the poised potential method using the redox couple Fe(dipyridyl)<sub>2</sub>Cl<sub>2</sub>/Fe(dipyridyl)<sub>2</sub>Cl<sub>3</sub> in 8 mM MES buffer (pH 5.3).<sup>25,26</sup> Oxidation of Fe(dipyridyl)<sub>2</sub>Cl<sub>2</sub> at each titration point

was followed by the decrease of absorbance at 522 nm ( $\epsilon_{522} = 5974 \text{ M}^{-1} \text{ cm}^{-1}$ ) until equilibrium was reached. Concentration of reduced laccase at equilibrium was considered to be  $\frac{1}{4}$  of the oxidized  $\text{Fe}(\text{dipyridyl})_2\text{Cl}_2$  concentration.

Marcus plots were obtained by representing  $\ln(k_x/k_H)$  versus  $\Delta G^\circ$ , calculated from the difference in redox potentials between the laccase and the different *p*-X-substituted phenols. Reorganization energies for electron transfer were calculated by fitting data to the following equation<sup>25</sup>:  $\ln(k_x/k_H) = \ln(k_B T/h) - \ln k_H - \Delta G^\ddagger / RT$ , where  $\Delta G^\ddagger = (\lambda/4)(1 + \Delta G^\circ/\lambda)^2$ .

### Synthesis of DAD

SA was dissolved in 80 mL of acetonitrile (27.5 mM concentration), and 80 mL of a 27.5 mM aqueous solution of  $\text{CuSO}_4$  was added. The mixture was stirred for 6 h at room temperature and evaporated to dryness at 40 °C under reduced pressure. The solid residue was redissolved in water and extracted with ethyl acetate. The organic layers were washed with brine, dried over anhydrous  $\text{Na}_2\text{SO}_4$ , and concentrated under vacuum to give the SA lactone dimer (308 mg, 0.69 mmol).<sup>27</sup> Crystallization from aqueous acetone yielded dilactone as yellow prisms (m.p. 212 – 214 °C, lit 208 °).<sup>28,29</sup> Structure was confirmed by NMR in acetone- $d_6$ .  $^1\text{H-NMR}$  spectrum (300 MHz),  $\delta$  (ppm): 7.60 (brs, 1H, OH), 6.74 (s, 4H), 5.76 (s, 2H), 4.12 (s, 2H) and 3.84 (s, 12H).  $^{13}\text{C-NMR}$  spectrum (75 MHz)  $\delta$  (ppm): 176.8, 149.7, 138.1, 130.6, 105.0, 84.2, 57.5 and 49.8.

### Systems setup for computational simulations

The initial structure was taken from the coordinates of PM1L (PDB 5ANH), which shares 98 % sequence identity with the chimeric variant 3A4. The 3A4 model contains a single mutation in the substrate binding pocket regarding PM1L (V162A), selected during the directed evolution of PM1L.<sup>6</sup> The C14F12 model additionally introduces F392N, while the CA32F1 model includes mutations V162R, T164E and F392N. In the first two proteins mutations were modeled with Maestro (version 10.0, Schrodinger, LLC, New York, NY, 2014), allowing for the modified amino acid and its neighbors (5 Å distance) to relax with IMPACT (version 6.5, Schrodinger, LLC, New York, NY, 2014). In the case of CA32F1 however, the introduction of a large side chain in position 162 (V to R) required further attention, and 20 ns of molecular dynamics (MD) simulation with DESMOND<sup>30</sup> was performed to assure the model's stability (see supplementary material).

The protonation state of titratable residues was estimated with the Protein Preparation Wizard (PROPKA) and the H++ server (<http://biophysics.cs.vt.edu/H++>), followed by visible inspection.<sup>31–33</sup> At pH 5 (in which most of the experiments were performed) histidines 55, 71, 91, 133, 153 and 401 were established to be fully protonated (positively charged); 66, 394 and 455 were  $\epsilon$ -protonated; and all others were  $\delta$ -protonated. Aspartic acids 50, 77, 101, 453 and 467 and glutamic acids 308 and 470 were also found to be protonated at pH 5. Further experiments were conducted at pH 3 and predicted  $\text{pK}_a$  values showed no changes in protonation states for both 3A4 and C14F12 (in particular in the binding pocket, where D205 is

found to have a  $\text{pK}_a$  of 1.2 and 1.8, respectively). In CA32F1, however, D205 has an increased  $\text{pK}_a$  of 3.8 and for this reason extra simulations for this system were also performed with protonated D205.

With an experimentally determined  $\text{pK}_a$  of 4.9,<sup>34</sup> SA is expected to have the protonated (SAH) and deprotonated ( $\text{SA}^-$ ) species in equilibrium at pH 5, and so all simulations have been performed with both models. Structures for SA, DAD and MS were fully optimized with Jaguar<sup>35</sup> in an implicit solvent and electrostatic potential charges computed with the density functional M06 at 6-31G\* level of theory. From these, ligand parameters were extracted for the classic simulations.

### PELE sampling

To sample the binding modes of the three computationally studied substrates (SA, DAD and MS) in the chimeric proteins, we have used the Protein Energy Landscape Exploration (PELE) software.<sup>36</sup> PELE is a Monte Carlo algorithm composed of a sequence of perturbation, relaxation, and a Metropolis acceptance test. In the first step, the ligand is subjected to random rotations and translations while the protein is perturbed based on the anisotropic network model (ANM).<sup>37</sup> For ligand perturbation the maximum allowed translation was 2.2 Å and the maximum rotation 20°. For the protein perturbation all atoms are displaced (a maximum of 0.5 Å) by moving  $\alpha$ -carbons to follow a random linear combination of the 6 lowest eigenvectors obtained in the ANM model. The relaxation step includes the repositioning of all amino acid side chains within 6 Å of the ligand and the 5 side chains with the highest energy increase along the previous ANM step. The relaxation stage ends with a truncated Newton minimization using the OPLS all-atom force field and an implicit surface-generalized Born continuum solvent.<sup>38,39</sup> New proposed minima are then accepted or rejected based on a Metropolis test. Substrate binding plots contain all accepted conformations for three 48 h-simulations using 40 processors.

### Quantum mechanics/molecular mechanics (QM/MM)

After applying an energy filter, randomly selected structures from PELE simulations were further optimized through five cycles of geometry optimization using Qsite,<sup>40</sup> and the atomic Mulliken spin density of the substrate was computed.<sup>41</sup> The protein is modelled classically using the OPLS force field while the substrate, the T1 copper atom, and residues H394, C450, H455, I452 and F460 are included in the quantum region. The density functional method employed was the M06-L functional, with the LANL2DZ effective core basis set for the copper atom and the 6-31G\* for all other atoms.<sup>42,43</sup>

## Results and Discussion

### Construction and screening of mutant libraries

Inspection of the molecular model for the parent 3A4 laccase revealed that the substrate binding pocket was delimited by amino acids in positions 162–164, 263, 264, 331, 336 and 390–392. In order to select the target residues for mutagenesis, we

## ARTICLE

## Journal Name

performed a multiple sequence alignment of laccases from fungi of the order Polyporales (including *P. cinnabarinus* and basidiomycete PM1) (Fig. 1). Residues in positions 162, 164, 263, 264, 390 and 392 (according to 3A4 laccase numbering) were the most variable and, therefore, were chosen for randomization. As simultaneous combinatorial saturation mutagenesis (CSM) of the six sites would imply screening more than  $10^9$  clones for 95 % library coverage, we used the ISM approach in order to diminish the screening effort.<sup>16</sup> In our case, we defined three regions, each comprising two target residues for mutagenesis: region A, for residues 162 and 164; region B, for residues 263 and 264; and region C, for residues 390 and 392. Individual libraries were constructed for each region and, this way, the number of clones to be screened for 95 % coverage was reduced to 3066 per library.

The mutant libraries were screened with SA at pH 5. This pH is described as the working pH for the enzymatic saccharification and yeast fermentation of prehydrolyzates from wheat straw biomass to produce ethanol.<sup>44</sup> Owing the common acidic pH of laccases, the availability of recombinant enzymes with more neutral optimum pH is of interest for biomass conversion processes. Activity landscapes of first generation mutant libraries A, B and C revealed different plasticity among regions, i.e., the admission of amino acidic variability in the selected positions (Fig. 2A). Region B was the least flexible of the three studied, with 83 % of clones presenting less than 5 % activity

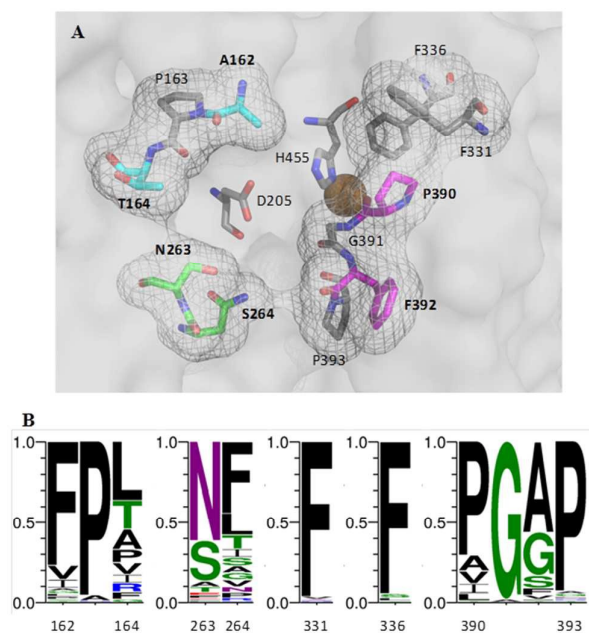


**Figure 1:** (A) Residues delimiting the substrate binding pocket of 3A4 laccase. Residues selected for mutagenesis are shown in cyan (region A), green (region B) and magenta (region C). Conserved residues His 455 and Asp 205, respectively involved in electron and proton transfer, are also shown. (B) Sequence logo for residues delimiting the substrate binding pocket in laccases of Polyporales. Heights indicate relative frequencies. Hydrophobic residues are shown in black, polar residues in green, acid residues in red, basic residues in blue and neutral residues in purple.

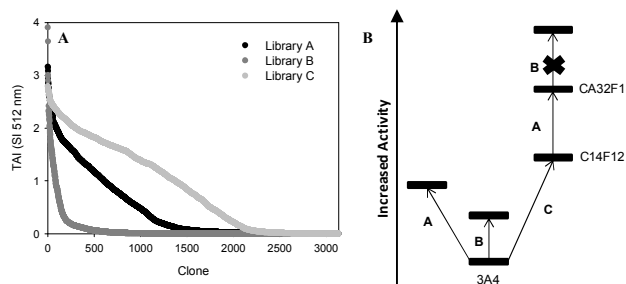


**Figure 2:** (A) Activity landscapes for mutant libraries A (black), B (dark grey) and C (light grey). (B) Representation of the ISM pathway followed in this work

respecting the parent laccase, followed by region A (48 %) and region C (29 %). The latter presented a high proportion of clones with better activity than parent type. A first re-screening was performed to rule out false positives, and plasmids from selected clones from each library were extracted and sequenced (Table S2). In the case of library A, the selected clones mutated A162 for polar residues. Notably, several included basic amino acids, even though the sequence alignment of laccases showed conserved hydrophobic residues in this position (mostly phenylalanine). All five clones from library B that were sequenced maintained N263, indicating its essential role for activity of these laccase variants (even though this position is quite variable among polyporal laccases). Finally, mutations in library C were the most variable, although the most frequent were the substitution F392N and the conservation of P390.

Next, a second re-screening, in which plasmids were re-transformed in yeast, was performed simultaneously for selected mutants from the three libraries. In general, total activity increase (TAI) values decreased in the order C > A > B, so the ISM pathway was defined as shown in Fig. 2B: the winner from library C would be used as scaffold for mutagenesis of region A (library CA), and the winner of this library would then be used as scaffold for the mutagenesis of region B (library CAB). In order to select the clone from library C to be used as parent for the next round of mutagenesis, ten clones showing the highest TAI values (2.5- to 4-fold higher than 3A4) were further subjected to a thermostability assay to discard any destabilizing mutations (Fig. S2). In general, we observed that clones that maintained P390 were the most stable. Hence, C14F12 mutant (F392N), with around 4-fold TAI and increased stability respecting 3A4 parent type, was selected as winner.

Activity landscape of library CA was similar to that observed for library A, although apparently the number of clones that retained parent activity was somewhat lower (Fig. S3A). Sequencing of selected clones revealed a possible epistatic relationship between mutations in region A and mutation F392N. This substitution seemed to favor the appearance of an acid-basic residue pair in positions 162 and 164 (Table S2), a bias that was not observed in library A. It is worth noting that available structures of fungal laccases co-crystallized with different substrates,<sup>45,46</sup> as well as site-directed mutagenesis

studies,<sup>17,47</sup> suggest that non-polar residues in these positions are essential for substrate-enzyme recognition, establishing hydrophobic interactions with the substrate's aromatic ring. This apparent contradiction could be explained by the increased polarity of the phenolic ring of SA due to the presence of two methoxyl groups, which could interact with the polar residues in positions 162 and 164.

As in the first generation, a thermostability screening was performed for selected clones from library CA, but no significant changes in stability were found. Therefore, the most active mutant CA32F1 (A162R/T164E/F392N) was selected as parent type for the third generation. In accordance to what was observed for libraries A and CA, activity landscape for library CAB was similar to library B, although maximum TAI values were not as high (Fig. S3B). Moreover, after screening over 5000 clones, DNA sequencing revealed that all clones selected held no new mutations.

### Biochemical characterization of selected ISM variants

Parent laccase 3A4 and variants C14F12 and CA32F1 were produced and purified to homogeneity for their characterization. While 3A4 and C14F12 presented  $T_{50}$  values of  $\sim 70$  °C, it decreased to 67 °C for CA32F1. ISM variants presented similar pH activity profiles for SA oxidation, more neutral compared to parent type (Fig. 3): optimum pH was 4 for all laccases, but the second best value (relative activity > 80 %) was obtained at pH 3 for 3A4 and at pH 5 for both C14F12 and CA32F1. This is a consequence of the selective pressure applied during library screening, performed at pH 5, as has been described in other laccase directed evolution studies.<sup>7,48–50</sup>

Concerning reaction kinetics for SA at pH 5 (Table I), ISM variants presented increased  $k_{cat}$  values, around 1.6-fold respecting parent type. Although these increments are not as high as desirable, it should be taken into account that SA is a natural substrate of fungal laccase and, hence, an enhancement of several folds in  $k_{cat}$  is difficult to achieve. For instance, during the active site re-design of a small bacterial laccase towards 2,6-dimethoxyphenol, several fold

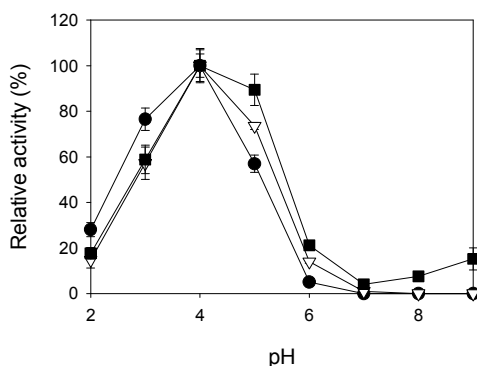


**Figure 3.** pH activity profiles with SA for laccase variants 3A4 (circles), C14F12 (triangles) and CA32F1 (squares). Means were obtained from triplicates, error bars represent standard deviations.

**Table I.** Kinetic constants for the oxidation of SA and DAD by the parent type laccase 3A4 and the ISM variants (C14F12 and CA32F1). Reactions at pH 5 were performed in 100 mM acetate buffer, while reactions at pH 3 were performed in 100 mM tartrate buffer.

Substrate		3A4	C14F12	CA32F1
SA (pH 5)	$k_{cat}$ ( $s^{-1}$ )	156 ± 3	251 ± 4	257 ± 3
	$K_m$ ( $\mu M$ )	7.0 ± 0.7	14.2 ± 0.7	9.9 ± 0.5
	$k_{cat}/K_m$	22 ± 3	17.7 ± 1.1	26 ± 2
SA (pH 3)	$k_{cat}$ ( $s^{-1}$ )	313 ± 8	338 ± 3	429 ± 9
	$K_m$ ( $\mu M$ )	92 ± 5	137 ± 13	80 ± 4
	$k_{cat}/K_m$	3.4 ± 0.3	2.5 ± 0.3	5.3 ± 0.4
DAD (pH 5)	$k_{cat}$ ( $s^{-1}$ )	68 ± 1	68 ± 3	73 ± 3
	$K_m$ ( $\mu M$ )	21.6 ± 1.3	59 ± 7	66 ± 9
	$k_{cat}/K_m$	3.2 ± 0.2	1.2 ± 0.2	1.1 ± 0.2

improvements were attained by punctual mutations, but the wild-type activity on this substrate was extremely low ( $k_{cat}$  0.87  $s^{-1}$ ).<sup>18</sup> Concerning  $K_m$ , C14F12 laccase presented a 2-fold increase respecting parent 3A4, whereas affinity was somewhat recovered in CA32F1. In all, catalytic efficiencies for SA at pH 5 are not significantly affected in the new variants. Nevertheless, it should be mentioned that, from an industrial point of view, the increase turnover rates is aimed, independently of the changes obtained in  $K_m$ , since substrate concentration does not represent a limiting factor in industrial enzymatic transformations (where high amounts of substrate are generally applied). It is also worth noting that despite the shifted pH activity profiles, CA32F1 still presents a higher turnover rate (and catalytic efficiency) towards SA than 3A4 parent type at pH 3.

In the HTS assay used for the screening of mutant libraries, oxidation of SA was followed by the development of a pinkish color ( $\lambda_{max}$  = 512 nm).<sup>23</sup> This colored product is a result of the oxidation of DAD, a phenolic dimeric compound formed from the  $\beta$ - $\beta'$  coupling of two phenoxyl radicals of SA, that is also a substrate for laccase (Scheme S1).<sup>47,51</sup> DAD was synthesized and the corresponding kinetic constants for its oxidation by the three laccase variants were obtained to verify whether TAI values observed in the library screenings were due to enhanced activity over SA alone or also to a better oxidation of DAD. Surprisingly,  $k_{cat}$  values were not enhanced, and affinity towards DAD was significantly worse for the ISM variants.

### Hammett and Marcus correlations

In order to ascertain whether mutations in ISM variants C14F12 and CA32F1 affected the reaction mechanism, Hammett and Marcus plots were obtained for the three laccases. Competition reactions at pH 5 with different  $p$ -X-substituted phenols ( $p$ -methoxyphenol,  $p$ -methylphenol,  $p$ -phenylphenol,  $p$ -chlorophenol and phenol) were carried out and  $\log(k_x/k_H)$  values were plotted against  $\sigma^+$  values for each substrate (Fig. S4A-C). Calculated  $\rho$ -values for the three laccases were all around -2 indicating that all three laccase variants are similarly dependent on the nature of the  $p$ -X-substituent group (Table II). These values are slightly lower than those obtained for other HRPLs from *Trametes villosa* and *Trametes versicolor*.<sup>25,52</sup> Redox potentials for the three laccases were also obtained, but no significant differences were found. The same occurred for total reorganization

## ARTICLE

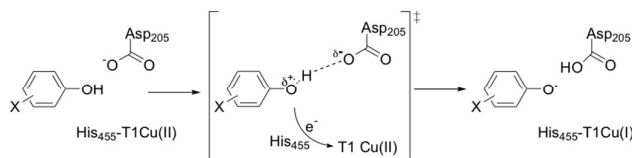
## Journal Name

**Table II.** Redox potentials (V vs NHE),  $\rho$ -values for Hammett plots and reorganization energies (kcal/mol) for Marcus plots calculated at pH 5 for 3A4 laccase and ISM variants (C14F12 and CA32F1).

Laccase	$E^0$	$\rho$ (Hammett)	$\lambda$ (Marcus)
<b>3A4</b>	0.7887 $\pm$ 0.0004	-1.9 $\pm$ 0.3	44.6 $\pm$ 0.3
<b>C14F12</b>	0.783 $\pm$ 0.002	-2.1 $\pm$ 0.2	47.4 $\pm$ 0.4
<b>CA32F1</b>	0.7752 $\pm$ 0.0006	-2.2 $\pm$ 0.1	45.6 $\pm$ 0.5

**Table III.** Average spin density (%) on the substrate at site 1 for the different QM/MM calculations. Standard deviations are indicated, as well as the proportion of structures corresponding to site 1 of all those evaluated.

	3A4		C14F12		CA32F1	
	Poses	Spin density (%)	Poses	Spin density (%)	Poses	Spin density (%)
<b>SAH</b>	0.95	88 $\pm$ 6	0.65	85 $\pm$ 5	0.89	83 $\pm$ 20
<b>SA<sup>-</sup></b>	0.33	87 $\pm$ 8	0.75	82 $\pm$ 10	0.95	86 $\pm$ 9
<b>DAD</b>	0.45	80 $\pm$ 8	0.69	88 $\pm$ 6	0.29	100 $\pm$ 1

**Scheme 1:** Concerted electron-proton transfer mechanism for the oxidation of phenols by 3A4 laccase and ISM variants.

energies ( $\lambda$ ) for electron transfer calculated according to Marcus equation (Fig. S4D-E), with values ranging from 45 to 47 kcal/mol (Table II), similar to those described for *T. villosa* and *T. versicolor* laccases.<sup>25,52</sup> Likewise to these two laccases, these results suggest that 3A4 laccase and ISM variants oxidize phenols by an asynchronous concerted electron-proton transfer mechanism, where the electron transfer to T1 copper site leads to the formation of a fleeting radical cation reactive intermediate (in agreement with the observed negative  $\rho$ -values) and the concomitant proton transfer to D205 residue leads to a phenoxyl radical product. This feature is appropriately described as an unbalanced transition state, according to Muller (Scheme 1).<sup>53</sup> In all, these results suggest that the selected mutations do not affect the mechanism of the reaction, and thus the increased turnover rates observed in the ISM laccase variants are caused by other factors.

#### Computational analysis of substrate binding and oxidation

To rationalize the effect of mutations on substrate oxidation, molecular simulations were performed.<sup>54</sup> The first step involved the identification of the main binding modes with PELE, which was performed for both protonation forms of SA (calculations were made at pH 5, Fig. 4). Then, SA oxidation was estimated through spin densities from QM/MM simulations (Table III). PELE results indicate that protonated SA (SAH) binds with higher affinity in the vicinity of the T1 site in 3A4 laccase (Fig. 4A): inspection of structures with interaction energy below -100 kcal/mol confirms that 19 out of 20 SAH binding modes were found inside the T1 cavity (hereafter named site 1, Fig. 5A). At this site the substrate's carboxylic acid is interacting with P393 and N207, while the phenolic group is surrounded by A162, P163 and the side chain of S264. In this site we find an average substrate spin density of 88%. For deprotonated SA (SA<sup>-</sup>), however, site 1 is less populated and a second minimum appears (Fig. 4B). Site 1 seen in Fig. 5B shows the substrate in a different orientation and further

away from the metal center due to the favorable interaction between the negatively charged carboxylate group and the backbone of G391 and F392 and the hydroxyl group of S387. Nevertheless, site 1 shows an average 87% spin density (although only one third of the analyzed structures correspond to this site), while the second minimum is less reactive (61% spin density, Table III). Furthermore, SA<sup>-</sup> is in average less protected from solvent than SAH, as seen by the higher solvent accessible surface area (SASA) at the best interaction energies. (Fig. S5). All these data indicate the preference of 3A4 laccase for SAH oxidation over SA<sup>-</sup>.

In C14F12, SAH presents two degenerate minima, at 7 Å and at 12 Å (Fig. 4C); both sites are also present in 3A4, although C14F12 has an increased population at the second minimum. Spin density for SAH at site 1 (85%) is similar to 3A4, but the second minimum shows reduced spin density (40%, Table III). Conversely, SA<sup>-</sup> binds mainly in site 1 (Fig. 4D). As in the case of 3A4, the substrate's carboxylate group interacts with the backbone of G391 and N392 and S387's side chain. However, mutation F392N causes the rotation of the backbone, creating a favorable binding site for the negatively charged substrate with the N392 side chain. Despite the anchored carboxylate group, the substrate's phenolic group shows two main orientations with different oxidation rates: inside the T1 Cu site, which is more frequent, interacting with P163 backbone and near D205 (93% spin density, Fig. 6A), or pointing directly to the solvent (48% spin density, Fig. 6B). These results suggest that the shifted pH activity profile and the improved activity seen at pH 5 for C14F12 ( $k_{\text{cat}} = 251 \text{ s}^{-1}$ ) relative to 3A4 ( $k_{\text{cat}} = 156 \text{ s}^{-1}$ ) could be mainly due to improved oxidation of SA<sup>-</sup>, which is more abundant at this pH than at pH 3. In agreement with this is the fact that the  $k_{\text{cat}}$  for 3A4 and C14F12 at pH 3 are very similar (313 and 338  $\text{s}^{-1}$ , respectively).

MD simulation performed for CA32F1 laccase (Fig. S6, S7) shows that R162 is mostly interacting with E164, but in ~25% of the time R162 is also interacting with D205, as a result of the flexibility observed in the loop hosting R162 and E164. Following MD relaxation, PELE simulations further confirmed the existence of these two conformations. For SAH, site 1 is highly populated (Fig. 4E) and two possible binding modes are observed: i) one very reactive (99% spin density) due to the favorable stacking of substrate between the two negatively charged residues (D205 and E164, Fig. 7A) and; ii) a less reactive one (75%) due to simultaneous interaction of D205,

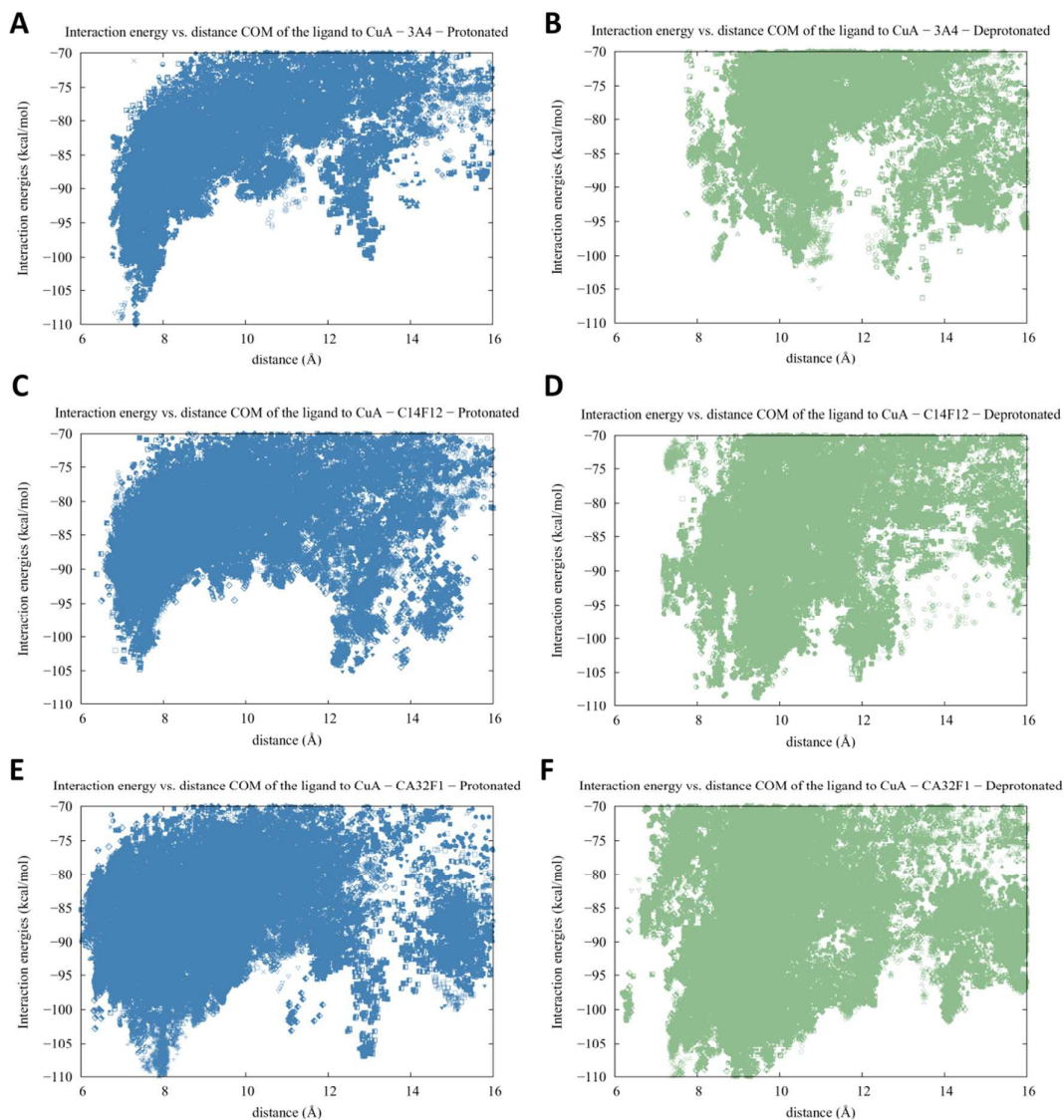


**Figure 4.** Interaction energy versus the T1copper–substrate (center of mass) distance for 3A4 (A,B), C14F12 (C,D) and CA32F1 (E,F) variants conformational search of SAH (A,C,E) and SA<sup>-</sup> (B,D,F).

R162 and E164 (**Fig. 7B**). In the case of SA<sup>-</sup>, again it is found almost exclusively in site 1 (**Fig. 4F**). In fact, 19 out of 20 structures were in this site with an average 86% spin density (**Table III**). SA<sup>-</sup> is anchored by G391, F392 and S387, similar to the most reactive binding mode found in C14F12, although not as well positioned due to the presence of the large side chain of R162. This indicates that the relative orientation of the side chains from R162, E164 and D205 affects the oxidation of the substrate. In fact, an arginine residue in the substrate binding pocket of CotA laccase has recently been described to be crucial for SA oxidation. The crystal structure reveals that its side-chain rotates 10° upon SA binding, sandwiching the substrate between itself and the T1 Cu site.<sup>55</sup> Finally, the SASA analysis shows a more buried interaction of the substrate at

the T1 copper site in CA32F1, particularly in the case of SAH (**Fig. S5E, F**).

We have also investigated the effect of lowering pH to 3 but predictions indicate that only CA32F1 could undergo changes in the binding pocket. With an estimated pK<sub>a</sub> of 3.8, D205 could be protonated, so calculations were repeated with SAH and both protonation states for D205. In this case PELE results indicate that SAH also binds in site 1, but the orientation of the ligand is different from that observed when D205 is not protonated. Also, low spin densities (18 – 65 %) are obtained when using the neutral form of D205, while values up to 100% are obtained for deprotonated D205. Hence, the improved catalytic efficiency of CA32F1 on SA at pH 3 can be attributed to the favorable oxidation of SAH (the dominant species at this



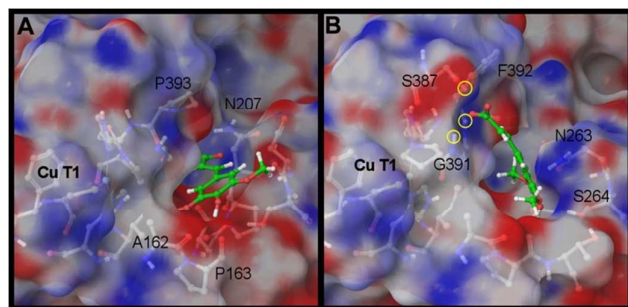


**Figure 5.** Representative binding modes for SA in 3A4. Panel A includes the most reactive mode for SAH while panel B corresponds to SA<sup>-</sup>. The main residues participating in the backbone amine site are identified with yellow circles.

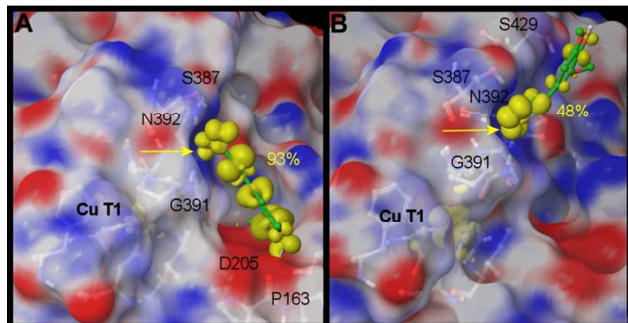


**Figure 6.** Representative binding modes for SA<sup>-</sup> with C14F12 protein. Panel A includes the most reactive mode (in yellow the spin density isosurface on the substrate) and panel B corresponds to a less active orientation with the carbonyl group exposed to the solvent. Arrows locate the carboxylate anchor point.

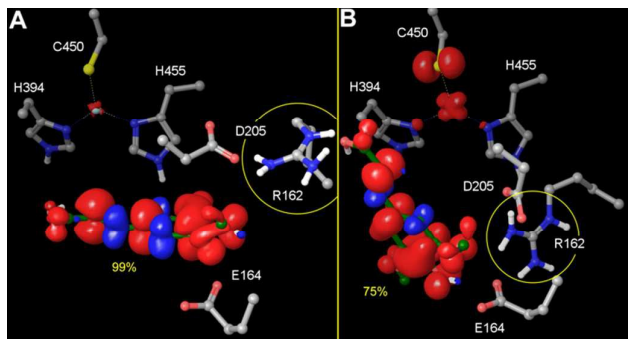


**Figure 7.** Representative protein-substrate complexes for CA32F1 and SAH. Spin density isosurfaces are shown in red and blue. In panel A an example of a conformation where the substrate is stacked between the two acids and B a less favorable oxidation position with simultaneous D205-R162-E164 interaction.

pH) and not to changes occurring in the protein. Although estimated  $pK_a$  show that catalytic D205 coexists in protonated and deprotonated forms in this variant at pH 3, binding SAH would displace the equilibrium, shifting D205 population towards the carboxylate form and allowing proton transfer from the substrate to the protein. Indeed, mutation of the equivalent residues for non-acidic amino acids in laccases from *T. versicolor* (D206A) and *Melanocarpus albomyces* (E235T) severely affected oxidation of phenolic substrates, especially at acidic pH.<sup>25,46,56</sup>

Taking all these results into account, we can conclude that the increased turnover rates for SA at pH 5 are caused by the enhanced oxidation of SA<sup>-</sup>, thanks to the anchoring of the substrate's carboxylate group by mutation F392N. However, in C14F12 variant this is at the expense of SAH oxidation. On the

other hand, CA32F1 is very active on both protonation forms of SA, presenting also increased  $k_{cat}$  at pH 3 respecting parent 3A4, although the relative position of the new acid-basic pair formed by R162 and E164 is determinant for efficient binding of the substrate.

Finally, simulations were also performed for DAD with the three proteins. They all presented more or less similar binding in site 1, although it's worth noting that in CA32F1 variant the interaction between R162 and E164 is observed in several structures, blocking the entrance of DAD into the substrate pocket. Overall, QM/MM results (Table III) are in agreement with the similar turnover rates obtained for DAD with the three laccases. CA32F1 variant showed up to 100% spin density, but due to the low proportion of site 1 structures used, these results were inconclusive.

### Oxidation of related syringyl-type phenols

We also evaluated the oxidation of other syringyl-type phenols (with two *o*-methoxyl substituents) by the three laccase variants, determining their kinetic constants towards methyl sinapate (MS), 2,6-dimethoxyphenol (DMP), syringic acid (SyA) and methyl syringate (MSy) at pH 5 (Table IV). These substrates, differing in the presence or not of a carboxylic group and the length of the aliphatic side chain, would help us understand the importance of the new binding mode created by mutation F392N, which was the sole responsible for the increased  $k_{cat}$  obtained towards SA in the first generation. The kinetic constants obtained for MS were similar to those of SA, with a 1.5-fold increase in  $k_{cat}$  and also in  $K_m$ , resulting in a similar efficiency among the different laccase variants. However, catalytic efficiencies for DMP, SyA and MSy were severely impaired due to similar  $k_{cat}$  values and an important increase in  $K_m$  values (3- to 7-fold respecting parent type). Additional simulations were performed to elucidate the improved oxidation of MS in C14F12. The minimum with highest spin density (ranging from 65 to 73 %) for parent 3A4 is very different from that found in variant C14F12 (with spin density ranging from 78 to 90 %, Fig. S9). In fact, C14F12 minima resemble the previously seen site 1 for SA<sup>-</sup>, with a favorable interaction between MS's carbonyl and the backbone of N392 and, more importantly, with the phenolic

**Table IV.** Kinetic constants for the oxidation of MS, DMP, SyA and MSy (pH 5).

Substrate	3A4	C14F12	CA32F1	
MS	$k_{cat}$ ( $s^{-1}$ )	195 ± 5	250 ± 5	309 ± 7
	$K_m$ ( $\mu M$ )	12.0 ± 1.1	16.0 ± 0.9	18.6 ± 1.2
	$k_{cat}/K_m$	16 ± 2	15.6 ± 1.2	16.6 ± 1.4
DMP	$k_{cat}$ ( $s^{-1}$ )	90 ± 1	131 ± 3	128 ± 2
	$K_m$ ( $\mu M$ )	46 ± 2	320 ± 30	191.7 ± 1.1
	$k_{cat}/K_m$	2.0 ± 0.1	0.41 ± 0.05	0.668 ± 0.014
SyA	$k_{cat}$ ( $s^{-1}$ )	57 ± 1	71 ± 3	63 ± 1
	$K_m$ ( $\mu M$ )	32.9 ± 2.5	189 ± 4	102 ± 5
	$k_{cat}/K_m$	1.7 ± 0.2	0.38 ± 0.02	0.61 ± 0.04
MSy	$k_{cat}$ ( $s^{-1}$ )	71 ± 2	66 ± 1	68 ± 1
	$K_m$ ( $\mu M$ )	132 ± 14	890 ± 30	710 ± 30
	$k_{cat}/K_m$	0.54 ± 0.07	0.082 ± 0.004	0.096 ± 0.005

group well positioned for proton abstraction at D205. This is not seen in 3A4, where the substrate is in a different orientation, probably due to steric hindrance of F392 on the extra methyl group. These results suggest that the opening of the T1 cavity by replacement of F392 by N could be the main responsible for the increased activity towards MS in C14F12, contributing also to the enhancement of SA oxidation. On the other hand, the lower catalytic efficiencies towards DMP, SyA and MSy shown by ISM variants suggest that the length of the side chain present in SA and MS could also be an important factor for favorable substrate binding in the engineered variants, providing better interaction between the phenolic group and D205. Indeed, in a related work we evaluated the oxidation of a battery of lignin-derived phenols by the selected laccase mutants from libraries A, B and C enumerated in **Table S2**. In this screening we observed a more pronounced increase in activity for mutants with F392N mutation towards SA, MS, ferulic acid and methyl ferulate than towards SyA, MSy, vanillic acid and methyl vanillate, respectively, which differ in the presence or not of the propenyl chain.<sup>57</sup>

## Conclusions

Combinatorial saturation mutagenesis on the substrate binding pocket together with experimental characterization and computational analysis of the resulting variants provided valuable information on the structural determinants for the oxidation of sinapic acid and related phenols by laccase. The results obtained put in evidence that the diversity of substrate binding pockets of fungal laccases in nature stands for the varied oxidation capabilities found in these generalist enzymes even if they hold similar redox potentials. Although the latter will be limiting the electron transfer between the substrate and the T1 copper, the binding event plays a crucial role in the overall rate of the reaction by creating an appropriate environment and substrate positioning that allows the oxidation to proceed. Concerning the engineering of laccases by rational design, it is shown that educated guesses may be misleading even for assessing the effect of a single mutation. The oxidation of each ligand is a unique combination of many factors. Thus, to engineer the enzyme, it is decisive to define the particular substrate and conditions for which the biocatalyst will be used, stressing the usefulness of atomic simulations in unveiling the molecular determinants for the efficient oxidation of a target molecule.

## Abbreviations

ABTS, 2,2'-azino-bis(3-ethylbenzothiazoline-6-sulfonic acid); CDS, coding DNA sequence; CSM, combinatorial saturation mutagenesis; DAD, dehydrodisinapic acid dilactone; DMP, 2,6-dimethoxyphenol; HRPL, high-redox potential laccase; ISM, iterative saturation mutagenesis; IVOE, in vivo overlap extension; MD, molecular dynamics; MS, methyl sinapate; MSy, methyl syringate; PELE, protein energy landscape exploration; QM/MM, quantum mechanics/molecular

mechanics; SA, sinapic acid; SAH, protonated SA; SA<sup>-</sup>, deprotonated SA; SASA, solvent-accessible surface area; SyA, syringic acid; TAI, total activity increase.

## Acknowledgements

This work was funded by INDOX (KBBE-2013-7-613549) European project and NOESIS (BIO2014-56388-R) and CTQ2013-48287-R Spanish National Projects. I.P. and G.S. acknowledge the Spanish Research Council (CSIC) and MINECO for their respective predoctoral fellowships.

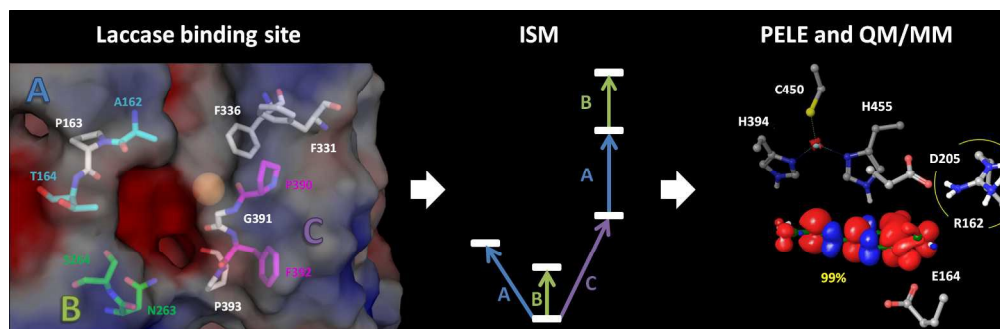
## References

- 1 S. Camarero, D. Ibarra, M. J. Martínez and A. T. Martínez, *Appl. Environ. Microbiol.*, 2005, **71**, 1775–1784.
- 2 S. Camarero, A. I. Cañas, P. Nousiainen, E. Record, A. Lomascolo, M. J. Martínez and A. T. Martínez, *Environ. Sci. Technol.*, 2008, **42**, 6703–6709.
- 3 A. I. Cañas and S. Camarero, *Biotechnol. Adv.*, 2010, **28**, 694–705.
- 4 S. Camarero, M. J. Martínez and A. T. Martínez, *Biofuels, Bioprod. Biorefining*, 2014, **8**, 615–625.
- 5 I. Pardo and S. Camarero, *Cell. Mol. Life Sci.*, 2015, **72**, 897–910.
- 6 D. Maté, C. García-Burgos, E. García-Ruiz, A. O. Ballesteros, S. Camarero and M. Alcalde, *Chem. Biol.*, 2010, **17**, 1030–1041.
- 7 S. Camarero, I. Pardo, A. I. Cañas, P. Molina, E. Record, A. T. Martínez, M. J. Martínez and M. Alcalde, *Appl. Environ. Microbiol.*, 2012, **78**, 1370–1384.
- 8 I. Pardo, A. I. Vicente, D. M. Mate, M. Alcalde and S. Camarero, *Biotechnol. Bioeng.*, 2012, **109**, 2978–2986.
- 9 M. Bunzel, J. Ralph, H. Kim, F. Lu, S. A. Ralph, J. M. Marita, R. D. Hatfield and H. Steinhart, *J. Agric. Food Chem.*, 2003.
- 10 N. Nićiforović and H. Abramovič, *Compr. Rev. Food Sci. Food Saf.*, 2014, **13**, 34–51.
- 11 A. Gaspar, M. Martins, P. Silva, E. M. Garrido, J. Garrido, O. Firuzi, R. Miri, L. Saso and F. Borges, *J. Agric. Food Chem.*, 2010, **58**, 11273–11280.
- 12 L. G. Landry, C. C. S. Chapple and R. L. Last, *Plant Physiol.*, 1995, **109**, 1159–1166.
- 13 M. Jurado, A. Prieto, Á. Martínez-Alcalá, Á. T. Martínez and M. J. Martínez, *Bioresour. Technol.*, 2009, **100**, 6378–6384.
- 14 A. D. Moreno, D. Ibarra, J. L. Fernández and M. Ballesteros, *Bioresour. Technol.*, 2012, **106**, 101–109.
- 15 A. D. Moreno, E. Tomás-Pejó, D. Ibarra, M. Ballesteros and L. Olsson, *Biotechnol. Biofuels*, 2013, **6**, 160.
- 16 M. T. Reetz and J. D. Carballreira, *Nat. Protoc.*, 2007, **2**, 891–903.
- 17 C. Galli, P. Gentili, C. Jolival, C. Madzak and R. Vadalà, *Appl. Microbiol. Biotechnol.*, 2011, **91**, 123–131.
- 18 M. D. Toscano, L. De Maria, S. Lobedanz and L. H. Østergaard, *ChemBioChem*, 2013, **14**, 1209–1211.
- 19 N. Gupta, F. S. Lee and E. T. Farinas, *J. Mol. Catal. B Enzym.*, 2010, **62**, 230–234.

## ARTICLE

## Journal Name

- 20 C. Notredame, D. G. Higgins and J. Heringa, *J. Mol. Biol.*, 2000, **302**, 205–217.
- 21 G. E. Crooks, G. Hon, J.-M. Chandonia and S. E. Brenner, *Genome Res.*, 2004, **14**, 1188–1190.
- 22 M. Alcalde, in *Methods in Molecular Biology*, ed. J. Braman, 2010, vol. 634, pp. 3–14.
- 23 I. Pardo, X. Chanagá, A. I. Vicente, M. Alcalde and S. Camarero, *BMC Biotechnol.*, 2013, **13**, 90.
- 24 E. García-Ruiz, D. Maté, A. Ballesteros, A. T. Martínez and M. Alcalde, *Microb. Cell Fact.*, 2010, **9**, 17.
- 25 C. Galli, C. Madzak, R. Vadalà, C. Jolivald and P. Gentili, *ChemBioChem*, 2013, **14**, 2500–2505.
- 26 F. Xu, W. Shin, S. H. Brown, J. A. Wahleithner, U. M. Sundaram and E. I. Solomon, *Biochim. Biophys. Acta - Protein Struct. Mol. Enzymol.*, 1996, **1292**, 303–311.
- 27 G. J. Fan, X. L. Jin, Y. P. Qian, Q. Wang, R. T. Yang, F. Dai, J. J. Tang, Y. J. Shang, L. X. Cheng, J. Yang and B. Zhou, *Chem. - A Eur. J.*, 2009, **15**, 12889–12899.
- 28 F. Lu and J. Ralph, *Org. Biomol. Chem.*, 2008, **6**, 3681–3694.
- 29 K. Freudenberg and H. Schraube, *Chem. Ber.*, 1955, **88**, 16–23.
- 30 D. Shivakumar, J. Williams, Y. Wu, W. Damm, J. Shelley and W. Sherman, *J. Chem. Theory Comput.*, 2010, **6**, 1509–1519.
- 31 G. Madhavi Sastry, M. Adzhigirey, T. Day, R. Annabhimoju and W. Sherman, *J. Comput. Aided. Mol. Des.*, 2013, **27**, 221–234.
- 32 M. H. M. Olsson, C. R. Søndergaard, M. Rostkowski and J. H. Jensen, *J. Chem. Theory Comput.*, 2011, **7**, 525–537.
- 33 R. Anandakrishnan, B. Aguilar and A. V. Onufriev, *Nucleic Acids Res.*, 2012, **40**, 537–541.
- 34 M. Ragnar, C. T. Lindgren and N.-O. Nilvebrant, *J. Wood Chem. Technol.*, 2000, **20**, 277–305.
- 35 A. D. Bochevarov, E. Harder, T. F. Hughes, J. R. Greenwood, D. A. Braden, D. M. Philipp, D. Rinaldo, M. D. Halls, J. Zhang and R. A. Friesner, *Int. J. Quantum Chem.*, 2013, **113**, 2110–2142.
- 36 K. W. Borrelli, A. Vitalis, R. Alcantara and V. Guallar, *J. Chem. Theory Comput.*, 2005, **1**, 1304–1311.
- 37 A. R. Atilgan, S. R. Durell, R. L. Jernigan, M. C. Demirel, O. Keskin and I. Bahar, *Biophys. J.*, 2001, **80**, 505–515.
- 38 G. A. Kaminski, R. A. Friesner, J. Tirado-Rives and W. L. Jorgensen, *J. Phys. Chem. B*, 2001, **105**, 6474–6487.
- 39 D. Bashford and D. A. Case, *Annu. Rev. Phys. Chem.*, 2000, **51**, 129–152.
- 40 R. B. Murphy, D. M. Philipp and R. A. Friesner, *J. Comput. Chem.*, 2000, **21**, 1442–1457.
- 41 R. S. Mulliken, *J. Chem. Phys.*, 1955, **23**, 1833.
- 42 P. J. Hay and W. R. Wadt, *J. Chem. Phys.*, 1985, **82**, 270.
- 43 W. J. Hehre, R. Ditchfield and J. A. Pople, *J. Chem. Phys.*, 1972, **56**, 2257–2261.
- 44 P. Alvira, A. D. Moreno, D. Ibarra, F. Sáez and M. Ballesteros, *Biotechnol. Prog.*, 2013, **29**, 74–82.
- 45 T. Bertrand, C. Jolivald, P. Briozzo, E. Caminade, N. Joly, C. Madzak and C. Mougin, *Biochemistry*, 2002, **41**, 7325–7333.
- 46 J. P. Kallio, S. Auer, J. Jänis, M. Andberg, K. Kruus, J. Rouvinen, A. Koivula and N. Hakulinen, *J. Mol. Biol.*, 2009, **392**, 895–909.
- 47 K. Koschorreck, S. M. Richter, A. Swierczek, U. Beifuss, R. D. Schmid and V. B. Urlacher, *Arch. Biochem. Biophys.*, 2008, **474**, 213–219.
- 48 T. Bulter, M. Alcalde, V. Sieber, P. Meinhold, C. Schlachtbauer and F. H. Arnold, *Appl. Environ. Microbiol.*, 2003, **69**, 987–995.
- 49 G. Festa, F. Autore, F. Fraternali, P. Giardina and G. Sannia, *Proteins*, 2008, 25–34.
- 50 P. Torres-Salas, D. M. Mate, I. Ghazi, F. J. Plou, A. O. Ballesteros and M. Alcalde, *ChemBioChem*, 2013, **14**, 934–937.
- 51 K. Lacki and Z. Duvnjak, *Biotechnol. Bioeng.*, 1998, **57**, 694–703.
- 52 M. A. Tadesse, A. D'Annibale, C. Galli, P. Gentili and F. Sergi, *Org. Biomol. Chem.*, 2008, **6**, 868.
- 53 P. Muller, *Pure Appl. Chem.*, 1994, **66**, 1077–1184.
- 54 E. Monza, M. F. Lucas, S. Camarero, L. C. Alejaldre, A. T. Martínez and V. Guallar, *J. Phys. Chem. Lett.*, 2015, **6**, 1447–1453.
- 55 T. Xie, Z. Liu, Q. Liu and G. Wang, *J. Struct. Biol.*, 2015, **190**, 155–161.
- 56 C. Madzak, M. C. Mimmi, E. Caminade, A. Brault, S. Baumberger, P. Briozzo, C. Mougin and C. Jolivald, *Protein Eng. Des. Sel.*, 2006, **19**, 77–84.
- 57 I. Pardo and S. Camarero, *Molecules*, 2015, **20**, 15929–15943.



196x63mm (300 x 300 DPI)